Hybrid photodetector is built for speed PAGE 80

LaserFocusWorld

MARCH 2008 WWW.LASERFOCUSWORLD.COM

INTERNATIONAL RESOURCE FOR TECHNOLOGY AND APPLICATIONS IN THE GLOBAL PHOTONICS INDUSTRY

PennWell

Nanoscale silicon yields chip-level modulators PAGE 61

researchers say, and then a 20 nm gold film and a spin-coated resist layer were deposited onto the sample. Finally, stacking alignment using gold alignment marks was applied to ensure accurate stacking of subsequent structure layers.

A key part of creating their 3-D metamaterial, the researchers note, was combining a planarization method for the rough nanolithography surface with robust alignment marks that survived the dry etching processes during nanofabrication. The resulting 3-D structures, created using the layer-by-layer method (which can be repeated as often as desired), consist of horseshoe-shaped gold nanowires arranged in a square pattern and perfectly stacked above each other (see Fig. 2). This method can produce arbitrary shapes in each layer as well, the group points out. And more complex structures such as twisted or chiral structures are also possible.

Investigating the interaction between adjacent SRRs, Giessen's group discovered it could control the electromagnetic coupling strength (which is related to spectral splitting of plasmon modes) by adjusting the vertical distance. The researchers believe the vertical interaction between metamaterial slabs can change the optical properties of metamaterials and lead to new characteristic spectral features with an increasing number of stacked layers. The resulting vertical coupling may prove beneficial in the design of broadband materials, and the group expects stronger coupling will lead to increased bandwidth.

Three-dimensional metamaterials possess highly desirable electromagnetic properties such as negative magnetic permeability and negative RIs, which will play a critical role in future applications like negative refraction, superlensing, and invisibility cloaking. Giessen's group believes the key to real-world applications will be balancing the number of stacked layers vs. intrinsic losses.

Sally Cole Johnson

REFERENCE
1. Na Liu et al., *Nature Materials*, DOI: 10.1038/nmat2072.

QUANTUM-RING LASERS

Whispering-cave-mode lasers emit in blue-violet

Lord Rayleigh wrote about the two-dimensional whispering gallery mode (WGM) in 1910 after a visit to the dome of St. Paul's cathedral in London. The whispering *cave* mode (WCM) is a three-dimensional (3-D) effect—a toroid with circular helix symmetry—which recent studies have shown can be used to create photonic-quantum-ring (PQR) lasers that emit in the blue-violet part of the spectrum.[1]

A research team at Pohang University of Science and Technology (POSTECH, Pohang, Korea) first created 3-D WCM lasers that emit in the infrared and red part of the spectrum. To achieve this, professor O'Dae Kwon and his group stacked mesas of vertically reflecting distributed-Bragg-reflector (DBR) structures above and below a few active 80 Å gallium arsenide and gallium indium phosphide quantum wells. The resulting 3-D WCM laser of photon-

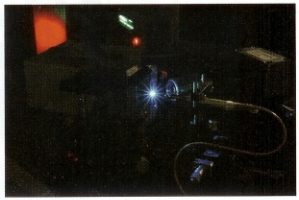

A blue photonic-quantum-ring laser showcases 3-D whispering-cave-mode emission with ultralow threshold current less than that of VCSELs or LEDs. (*Courtesy of Odae Kwon, POSTECH*)

ic quantum rings avoided the problem of in-plane light spreading found in 2-D WGM lasers, and generated a doughnut-like band of 3-D helical modes. One such photonic-quantum-ring device 15 μm in diameter featured an ultralow threshold current of 11.5 μA, about a thousandth of that needed for vertical-cavity surface-emitting lasers (VCSELs) of the same diameter. These multimode devices emitted around a central wavelength of 848 nm, exhibiting increasing threshold current and decreasing linewidth with larger device diameter. The team observed the narrowest linewidth with an optical spectrum analyzer to date from a 10 μm PQR of 0.55 Å at an injection current of 800 μA.

The next iterations of the infrared PQR device involved single-mode electrically pumped lasers made of a hyperboloid drum shape only 0.9 μm across. These devices exhibited a linewidth of 0.46 Å at 838.5 μm, and a tiny threshold current of 300 nA, the smallest ever observed among quantum-well, wire, or dot-type lasers. Although the external quantum efficiency suffered from soft lasing turn-on behavior, the emission efficiency of the PQR laser was very high—more favorable than that of light-emitting diodes (LEDs). Such lasers could be used to replace LEDs in high-end displays in the near future.

The researchers then used various vertical gallium nitride (GaN) structures to extend their PQR work to blue wavelengths from 420 to 470 nm (see figure). In one version, a "reverse-mesa" approach with microholes etched in the vertical-quantum-well structure enabled unexpected "convex whispering-gallery" lasing via gain-guiding effects. This "weird" laser also exhibited very low quantum-ring-like thresholds (6 μA per pixel for 256 × 256 arrays, and 0.3 μA per pixel for megapixel arrays at room temperature) and surface-normal dominant multimode emissions. The hole lasers are easily fabricated, readily scalable, and, says Kwon, may become sought-after for next-generation interconnects or nanobioengineering for their potential to anchor submicron fibers.

THIS "WEIRD" LASER ALSO EXHIBITED VERY LOW QUANTUM-RING-LIKE THRESHOLDS AND SURFACE-NORMAL DOMINANT MULTIMODE EMISSIONS.

"In general," said Kwon, "the blue laser has been like a 'holy grail'—it has been very difficult to achieve surface-normal lasing. Existing blue photonic-crystal laser diodes still require relatively high current. The new blue PQR achieves surface-normal lasing easily, even with the modest design of less than 95% to 70% vertical-pair reflection, thanks to the unique 3-D helix WCM phenomena. And its ultralow threshold implies it can outperform LEDs while overcoming the thermal and material problems of the LED."

Future challenges associated with 3-D WCM PQR lasers include studies of 3-D device theory and simulations, angular moment studies, understanding of carrier-photon interactions, and chaotic dynamics research on modified structures.

Valerie C. Coffey

REFERENCES

1. O. Kwon et al., *Proc. SPIE Photonics West*, 6872, (2008).

$$\frac{dA_s^{(-)}}{dz}\,e^{i(\omega t+\beta_s z)} - \frac{dA_s^{(+)}}{dz}\,e^{i(\omega t-\beta_s z)} - \text{c.c.}$$

$$= -\frac{i}{2\omega}\frac{\partial^2}{\partial t^2}\int_{-\infty}^{\infty}[P_{\text{pert}}(\mathbf{r},t)]_y \mathcal{E}_y^{(s)}(x)\,dx \qquad (13.3\text{-}9)$$

The presence of two terms on the left side of Equation (13.3-9) is due to the fact that the summation over m in (13.3-8) contains two terms involving $\mathcal{E}_y^{(m)}(x)$ for each value of m—one, designated as $(-)$, traveling in the $-z$ direction, and the other $(+)$, traveling in the $+z$ direction.

Equation 13.3-9 can be used to treat a large variety of mode interactions [12]. Each physical example involves, in general, a different perturbation polarization $\mathbf{P}_{\text{pert}}(\mathbf{r}, t)$. They all, however, lead to the same set of "coupled mode" equations of the form of Equation (13.5-1). Some important examples are considered in the following sections.

13.4 PERIODIC WAVEGUIDE

Consider a periodic dielectric waveguide in which the periodicity is due to a corrugation of one of the interfaces as shown in Figure 13-6. Such periodic waveguides are used for optical filtering [16] as well as in the distributed feedback laser [17–19]. These two applications will be described further below.

The corrugation is described by the dielectric perturbation $\Delta\varepsilon(\mathbf{r}) \equiv \varepsilon_0\Delta n^2(\mathbf{r})$ such that the total dielectric constant is

$$\varepsilon'(\mathbf{r}) = \varepsilon(\mathbf{r}) + \Delta\varepsilon(\mathbf{r})$$

The perturbation polarization is from (13.3-2) and (13.3-3)

$$\mathbf{P}_{\text{pert}}(\mathbf{r}, t) = \Delta\varepsilon(\mathbf{r})\mathbf{E}(\mathbf{r}, t) = \Delta n^2(\mathbf{r})\varepsilon_0\mathbf{E}(\mathbf{r}, t) \qquad (13.4\text{-}1)$$

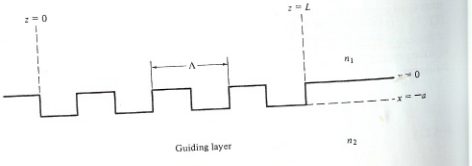

Figure 13-6 A corrugated periodic waveguide.

Since $\Delta n^2(\mathbf{r})$ is a scalar, it follows, from (13.3-4), that the corrugation couples only TE to TE modes and TM to TM, but not TE to TM.

To be specific consider TE mode propagation. Using (13.3-5) in (13.4-1) gives

$$[P_{\text{pert}}(\mathbf{r}, t)]_y = \frac{\Delta n^2(\mathbf{r})\varepsilon_0}{2}\sum_m [A_m\mathcal{E}_y^{(m)}(x)e^{i(\omega t-\beta_m z)} + \text{c.c.}] \qquad (13.4\text{-}2)$$

which, when used in (13.3-9), leads to

$$\frac{dA_s^{(-)}}{dz}\,e^{i(\omega t+\beta_s z)} - \frac{dA_s^{(+)}}{dz}\,e^{i(\omega t-\beta_s z)} - \text{c.c.}$$

$$= -\frac{i\varepsilon_0}{4\omega}\frac{\partial^2}{\partial t^2}\sum_m\left[A_m\int_{-\infty}^{\infty}\Delta n^2(x, z)\mathcal{E}_y^{(m)}(x)\mathcal{E}_y^{(s)}(x)\,dx e^{i(\omega t-\beta_m z)} + \text{c.c.}\right] \qquad (13.4\text{-}3)$$

We may consider the right side of (13.4-3) as a source wave term driving the forward wave $A_s^{(+)}\exp[i(\omega t - \beta_s z)]$ and the backward wave $A_s^{(-)}\exp[i(\omega t + \beta_s z)]$ on the left side. In order for a wave to be driven by a source, both source wave and driven wave must have the same frequency so that the interaction will not average out to zero over a long time (long compared to a period of their difference frequency). Equally important: Both source and wave need to have nearly the same phase dependence $\exp(i\beta z)$ so that the interaction does not average out to zero with distance of propagation z. If, for example, it is desired that the forward wave $A_s^{(+)}\exp[i(\omega t - \beta_s z)]$ be excited, it is necessary that at least one term on the right side of (13.4-3), say the lth one, vary as $\exp[i(\omega t - \beta z)]$ with $\beta \approx \beta_s$. If no other terms on the right side of (13.4-3) satisfy this condition, we simplify the equation by keeping only the forward wave on the left side and the lth on the right. We describe this situation by saying that the perturbation $\Delta n^2(x, z)$ couples the forward $(+s)$ mode to the lth mode and vice versa.

To be specific, let us assume that the period Λ in the z direction of the perturbation $\Delta n^2(x, z)$ is so chosen that $l\pi/\Lambda \approx \beta_s$ for some integer l. We can expand $\Delta n^2(x, z)$ of a square wave perturbation as a Fourier series

$$\Delta n^2(x, z) = \Delta n^2(x)\sum_{q=-\infty}^{\infty} a_q e^{i(2q\pi/\Lambda)z} \qquad (13.4\text{-}4)$$

The right side of (13.4-3) now contains a term $(q = l,\ m = s)$ proportional to $A_s^{(+)}\exp[i(2l\pi/\Lambda - \beta_s)z]$. But

$$\frac{2l\pi}{\Lambda} - \beta_s \approx \beta_s$$

so that this term is capable of driving synchronously the amplitude $A_s^{(-)}\exp(i\beta_s z)$ on the left side of (13.4-3) with the result

$$\frac{dA_s^{(-)}}{dz} = \frac{i\omega\varepsilon_0}{4}A_s^{(+)}\int_{-\infty}^{\infty}\Delta n^2(x)[\mathcal{E}_y^{(s)}(x)]^2\,dx a_l e^{i[(2l\pi/\Lambda)-2\beta_s]z} \qquad (13.4\text{-}5)$$

The coupling between the backward $A_s^{(-)}$ and the forward $A_s^{(+)}$ by the lth harmonic of $\Delta n^2(x, z)$ can thus be described by

$$\frac{dA_s^{(-)}}{dz} = \kappa A_s^{(+)} e^{-i2(\Delta\beta)z} \tag{13.4-6}$$

and reciprocally

$$\frac{dA_s^{(+)}}{dz} = \kappa^* A_s^{(-)} e^{i2(\Delta\beta)z}$$

where

$$\kappa = \frac{i\omega\varepsilon_0 a_l}{4} \int_{-\infty}^{\infty} \Delta n^2(x) [\mathcal{E}_y^{(t)}(x)]^2 \, dx \tag{13.4-7}$$

$$\Delta\beta \equiv \beta_s - \frac{l\pi}{\Lambda} \equiv \beta_s - \beta_0 \tag{13.4-8}$$

Some General Properties of the Coupled Mode Equations

The coupled mode equations (13.4-6), first encountered here, play a major role in guided wave optics [12]. They describe not only coupling between modes due to a spatially periodic index perturbation but also, as we shall show later, many other situations, including electrooptic and acoustooptic coupling between modes in neighboring waveguides and within the same waveguide. It is thus worthwhile to pause and consider some of the basic properties of these equations, which are independent of the specific application.

To simplify our notation, we replace the amplitude $A_s^{(-)}$ of the backward propagating mode by A, and that of the forward mode by B. The coupled mode equations (13.4-6) now read

$$\frac{dA}{dz} = \kappa_{ab} B \exp[-i2(\Delta\beta)z] \tag{13.4-9}$$

$$\frac{dB}{dz} = \kappa_{ba} A \exp[i2(\Delta\beta)z]$$

$$2(\Delta\beta) \equiv |\beta_b| + |\beta_a| - \ell\frac{2\pi}{\Lambda} \qquad \ell = 1, 2, 3 \cdots \tag{13.4-9a}$$

$$\kappa_{ba} = \kappa_{ab}^*$$

for modes carrying power in *opposite* directions. The phase of κ_{ab} is immaterial since it depends, according to Equation (13.4-4, 5), on the arbitrary choice of our $z = 0$ reference plane. It follows straightforwardly from (13.4-9) that

$$\frac{d}{dz}(|B(z)|^2 - |A(z)|^2) = 0 \tag{13.4-9b}$$

13.5 COUPLED-MODE SOLUTIONS

Let us return to the coupled-mode equations (13.4-6). For simplicity let us put $A_s^{(-)} \equiv A$, $A_s^{(+)} \equiv B$ and write them as

$$\frac{dA}{dz} = \kappa_{ab} B e^{-i2(\Delta\beta)z}$$

$$\frac{dB}{dz} = \kappa_{ab}^* A e^{+i2(\Delta\beta)z} \tag{13.5-1}$$

$\ell = 0, \pm 1, \pm 2, \ldots$

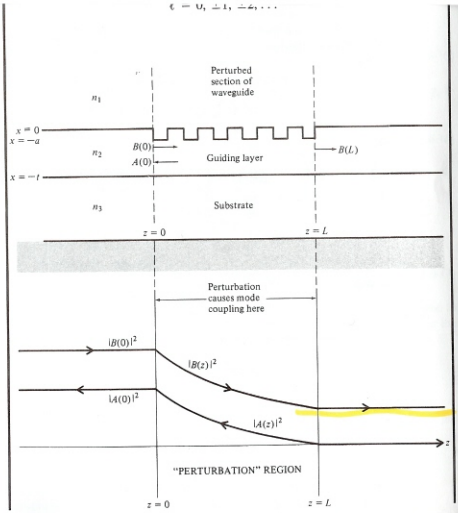

Figure 13-7 (*upper*) A corrugated section of a dielectric waveguide. (*lower*) The incident and reflected intensities inside the corrugated section.

Consider a waveguide with a corrugated section of length L as in Figure 13-6. A wave with an amplitude $B(0)$ is incident from the left on the corrugated section.

The solution of (13.5-1) for this case subject to $A(L) = 0$ is

$$A(z)e^{i\beta z} = B(0)\frac{i\kappa_{ab}e^{i\beta_0 z}}{-\Delta\beta\sinh SL + iS\cosh SL}\sinh[S(z-L)]$$

$$B(z)e^{-i\beta z} = B(0)\frac{e^{-i\beta_0 z}}{-\Delta\beta\sinh SL + iS\cosh SL} \times\{\Delta\beta\sinh[S(z-L)] + iS\cosh[S(z-L)]\} \quad (13.5\text{-}2)$$

where

$$S = \sqrt{\kappa^2 - (\Delta\beta)^2}$$
$$\kappa \equiv |\kappa_{ab}| \quad (13.5\text{-}3)$$

Under the matching condition $\Delta\beta = 0$, we have

$$A(z) = B(0)\frac{\kappa_{ab}}{\kappa}\frac{\sinh[\kappa(z-L)]}{\cosh\kappa L}$$
$$B(z) = B(0)\frac{\cosh[\kappa(z-L)]}{\cosh\kappa L} \quad (13.5\text{-}4)$$

A plot of the mode powers $|B(z)|^2$ and $|A(z)|^2$ for this case is shown in Figure 13-7. For sufficiently large arguments of the cosh and sinh functions in (13.5-4), the incident mode power drops off exponentially along the perturbation region. This behavior, however, is due not to absorption but to *reflection* of power into the backward traveling mode, A.

From (13.3-5) and (13.5-2) we find that the z-dependent parts of the wave solutions in the periodic waveguide are exponentials with propagation constants

$$\beta' = \beta_0 \pm iS = \frac{l\pi}{\Lambda} \pm i\sqrt{\kappa^2 - [\beta(\omega) - \beta_0]^2} \quad (13.5\text{-}5)$$

where we used $\Delta\beta \equiv \beta - \beta_0$, $\beta_0 \equiv \pi l/\Lambda$.

We note that for a range of frequencies such that $\Delta\beta(\omega) < \kappa$, β' has an imaginary part. This is the so-called "forbidden" region in which the evanescence behavior shown in Figure 13-7 occurs and which is formally analogous to the energy gap in semiconductors where the periodic crystal potential causes the electron propagation constants to become complex. Note that for each value of l, $l = 1, 2, 3 \ldots$, there exists a gap whose center frequency ω_{0l} satisfies $\beta(\omega_{0l}) = l\pi/\Lambda$. The exceptions are values of l for which κ is zero. We can approximate $\beta(\omega)$ near its Bragg value $(\pi l/\Lambda)$ by $\beta(\omega) \approx (\omega/c)n_{\text{eff}}$ (n_{eff} is an effective index of refraction). The result is

$$\beta' \cong \frac{l\pi}{\Lambda} \pm i\left[\kappa^2 - \left(\frac{n_{\text{eff}}}{c}\right)^2(\omega - \omega_{0l})^2\right]^{1/2} \quad (13.5\text{-}6)$$

where ω_{0l}, the midgap frequency, is the value of ω for which the unperturbed β is equal to $\beta_0 = l\pi/\Lambda$.

A plot of Re β' and Im β' (for $l = 1$) versus ω, based on (13.5-6), is shown in Figure 13-8. We note that the height of the "forbidden" frequency zone is

$$(\Delta\omega)_{\text{gap}} = \frac{2\kappa c}{n_{\text{eff}}} \quad (13.5\text{-}7)$$

where κ is according to (13.4-17) a function of the integer l. It follows from (13.5-6) that

$$(\text{Im }\beta')_{\max} = \kappa \quad (13.5\text{-}8)$$

In solid-state physics, it is well known that the behavior of electrons is described by means of electron wave functions that are of the form

$$\Psi_l = u_l(\mathbf{r})\exp\left(-i\frac{E_l t}{\hbar} + ik_l\cdot\mathbf{r}\right)$$

There exist regions of electron energy E_l where the propagation constant k is complex independently of the direction of k_l in complete formal analogy with (13.5-6). These are the so-called *forbidden energy gaps* of the crystal. Recent proposals and experiments [16,22] suggest that it should be possible to engineer "optical crystals" that have a three-dimensional periodicity that will possess a forbidden frequency gap for which optical propagation will be evanescent (i.e., with a complex propagation constant that is a three-dimensional generalization of (13.5-6)).

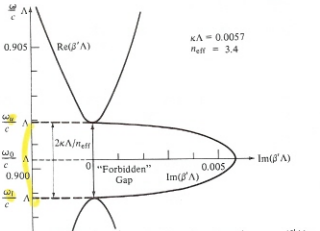

Figure 13-8 Dependence of the real and imaginary parts of the mode propagation constant, β', of the modes in a periodic waveguide. At frequencies $\omega_1 < \omega < \omega_u$, Im($\beta'$) $\neq 0$ and the modes are evanescent. At these frequencies, Re $\beta' = l\pi/\Lambda$.

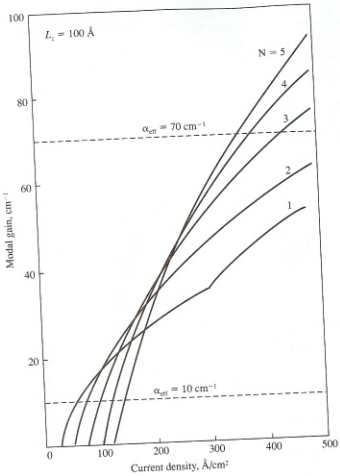

Figure 16-6 The modal gain $g_{mod}(= \Gamma g)$ as a function of the injected current with the number N of quantum wells as a parameter. (After Reference [3].)

index region. This graded index (and graded energy gap) region is grown by tapering the Al concentration from 0% to 60% in a gradual fashion as shown. The graded region functions as both a dielectric waveguide and as a funnel for the injected electrons and, not shown, the holes, herding them into the quantum well.

16.3 DISTRIBUTED FEEDBACK LASERS (9, 10, 11)

All laser oscillators employ optical feedback. By the word *feedback* we mean a means for ensuring that part of the optical field passing through a given point returns to the point repeatedly. If the delay is equal to an integral number of optical periods, this leads, in the presence of gain, to a sustained self-consistent oscillating mode

where the field stimulated by atoms at any moment adds up coherently and *in phase* to those emitted earlier. In the laser resonators studied so far in this book, the feedback was provided by two oppositely facing reflectors. Feedback can also be achieved in a traveling wave folded-path geometry.

In distributed feedback (DFB) lasers, the reflection feedback of forward into backward waves, and vice versa, takes place not at the end reflectors but continuously throughout the length of the resonator. This coupling is due to a spatially periodic modulation of the index of refraction of the medium or of its optical gain. These lasers enjoy a wavelength stability that is far superior to those of ordinary Fabry–Perot lasers. This stability is due to the fact that the laser mode prefers to oscillate at a frequency such that the spatial period Λ of the index perturbation is equal to some (usually small) integer (ℓ) number of guide half wavelengths:

$$\Lambda = \ell \frac{\lambda_g}{2} \left(\lambda_g = \frac{2\pi}{\beta} \right) \qquad \ell = 1, 2, 3, \ldots$$

where β is the propagation constant of the optical field in the waveguide. This condition, which ensures that reflections from different unit cells of the periodic perturbation add up in phase, is referred to as the *Bragg condition*. This is in analogy with the, formally similar, phenomenon of x-ray diffraction from the periodic lattice of crystals. This enables the laser designer, through a choice of Λ, to "force" the laser to oscillate at any predetermined wavelength, provided that the amplifying medium is capable of providing sufficient gain at that wavelength. This property is especially important in semiconductor lasers used in optical fiber communication. Such lasers are often required to operate within narrow, prescribed wavelength regions to minimize pulse spreading by chromatic (group velocity) dispersion or to avoid crosstalk from other laser beams at different wavelengths sharing the same fiber.

We will start our treatment of the distributed feedback (DFB) laser with a derivation of the relevant coupled mode equations. The essence of the DFB laser is a spatially periodic waveguide *with gain*. It is thus described by the coupled-mode equations (13.5-1) with the addition of gain terms

$$\frac{dA}{dz} = \kappa_{ab} e^{-2i(\Delta\beta)z} - \gamma A$$

$$\frac{dB}{dz} = \kappa_{ab}^* e^{2i(\Delta\beta)z} + \gamma B \qquad \text{(16.3-1)}$$

$$\Delta\beta \equiv \beta - \beta_0 = \beta - \frac{\pi}{\Lambda} \qquad \text{for } \ell = 1 \qquad \text{(16.3-2)}$$

We shall choose, without loss of generality, a real κ so that $\kappa_{ab} = \kappa_{ba}^* \equiv \kappa$. The gain terms, $-\gamma A$ and γB, are chosen such that if, hypothetically, we eliminate the periodic perturbation ($\kappa = 0$), the waves A and B are uncoupled and grow exponentially, each along its direction of propagation as $\exp(\gamma \times \text{distance})$. We could, of course, have derived Equations (16.3-1) by including *ab initio* gain in the derivation

leading to Equations (13.5-1).[2] Equations (16.3-2) can be simplified by defining new complex amplitudes $A'(z)$ and $B'(z)$

$$A(z) = A'(z)\exp(-\gamma z)$$
$$B(z) = B'(z)\exp(\gamma z) \tag{16.3-4}$$

The result is

$$\frac{dA'}{dz} = \kappa_{ab} B' e^{-i2(\Delta\beta + i\gamma)z} \tag{16.3-5}$$

$$\frac{dB'}{dz} = \kappa_{ab}^* A' e^{i2(\Delta\beta + i\gamma)z} \tag{16.3-6}$$

These equations are identical in form to those of (13.5-1), provided we replace in the latter, $\Delta\beta \rightarrow \Delta\beta + i\gamma$. We can thus use the solution (13.5-2) of Equations (13.5-1) to write down directly the solutions for the complex amplitudes $E_i(z)$ and $E_r(z)$ of the incident and reflected waves, respectively, *inside* the *amplifying* periodic waveguide. We take the boundary conditions to be those of a *single* right-traveling wave incident from the left with an amplitude $B(0)$. The solution of Equations (16.3-5, 6) in this case is

$$E_i(z) = B'(z)e^{[(-i\beta+\gamma)z]} = B(0)\frac{e^{-i\beta_0 z}[(\gamma - i\Delta\beta)\sinh[S(L-z)] - S\cosh[S(L-z)]]}{(\gamma - i\Delta\beta)\sinh(SL) - S\cosh(SL)} \tag{16.3-7}$$

$$E_r(z) = A'(z)e^{[(i\beta-\gamma)z]} = B(0)\frac{\kappa_{ab}e^{i\beta_0 z}\sinh[S(L-z)]}{(\gamma - i\Delta\beta)\sinh(SL) - S\cosh(SL)} \tag{16.3-8}$$

$$S^2 = |\kappa|^2 + (\gamma - i\Delta\beta)^2 \tag{16.3-9}$$

The fact that S now is complex makes for a major qualitative difference between the behavior of the passive periodic guide (13.5-2) and the periodic guide with gain. To demonstrate this difference, consider the case when the condition

$$(\gamma - i\Delta\beta)\sinh SL = S\cosh SL \tag{16.3-10}$$

is satisfied. It follows from (16.3-7, 8) that both the reflectance, $E_r(0)/E_i(0)$, and the transmittance, $E_i(L)/E_i(0)$, become infinite. *The device acts as an oscillator*, since it yields finite output fields $E_r(0)$ and $E_i(L)$ with no input $[E_i(0) = 0]$. Condition (16.3-10) is thus the oscillation condition for a distributed feedback laser. For the case of $\gamma = 0$, it follows, from (13.5-2), that $|E_i(L)/E_i(0)| < 1$, and $|E_r(0)/E_i(0)| < 1$ as appropriate to a passive device with no internal gain.

For frequencies very near the Bragg frequency $\omega_0(\Delta\beta \cong 0)$ and for sufficiently

[2] This can be done formally by replacing the real dielectric constant $\epsilon(\mathbf{r})$ in (13.3-3) by a complex $\epsilon_c(\mathbf{r})$: $\epsilon_c(\mathbf{r}) = \epsilon_r(\mathbf{r}) + i\epsilon_i(\mathbf{r})$. For the case of a uniform $\epsilon_i(\mathbf{r}) = \epsilon_i$, we obtain $\gamma = \omega\sqrt{\mu\epsilon_r\epsilon_i}$. Otherwise γ involves a spatial integral (see Problem 16.6).

high-gain constant γ so that (16.3-10) is nearly satisfied, the guide acts as a high-gain amplifier. The amplified output is available either in reflection with a field gain

$$\frac{E_r(0)}{E_i(0)} = \frac{\kappa_{ab}\sinh SL}{(\gamma - i\Delta\beta)\sinh SL - S\cosh SL} \tag{16.3-11}$$

or in transmission with a gain

$$\frac{E_i(L)}{E_i(0)} = \frac{-Se^{i\beta_0 L}}{(\gamma - i\Delta\beta)\sinh SL - S\cosh SL} \tag{16.3-12}$$

The behavior of the incident and reflected field for a high-gain case is sketched in Figure 16-7. Note the qualitative difference between this case and the passive (no gain) one depicted in Figure 13-7.

The reflection power gain, $|E_r(0)/E_i(0)|^2$, and the transmission power gain $|E_i(L)/E_i(0)|^2$, are plotted in Figure 16.8 as a function of $\Delta\beta$ and γ. Each plot contains four infinite gain singularities at which the oscillation condition (16.3-10) is satisfied. These are four longitudinal laser modes. Higher orders exist but are not shown.

Oscillation Condition

The oscillation condition (16.3-10) can be written as

$$\frac{S - (\gamma - i\Delta\beta)}{S + (\gamma - i\Delta\beta)}e^{2SL} = -1 \tag{16.3-13}$$

In general, one has to resort to a numerical solution to obtain the threshold values of $\Delta\beta$ and γ for oscillation [17]. In some limiting cases, however, we can

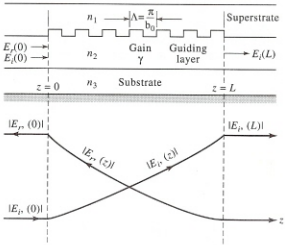

Figure 16-7 Incident and reflected fields inside an amplifying periodic waveguide.

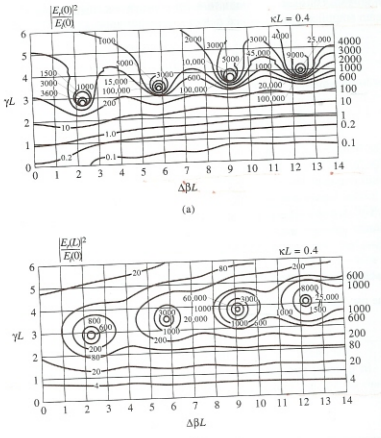

Figure 16-8 (a) Reflection gain contours in the $\Delta\beta L - \gamma L$ plane. $\Delta\beta$ is defined by (16.3-2) and is proportional to the deviation of the frequency $\omega_0 = \pi c/\Lambda n$. The plots are symmetric about $\Delta\beta$, so that only one-half ($\Delta\beta > 0$) of the plots is shown. (b) Transmission gain. [Courtesy of H. W. Yen.]

obtain approximate solutions. In the high-gain $\gamma \gg \kappa$ case, we have from the definition of $S^2 = \kappa^2 + (\gamma - i\Delta\beta)^2$

$$S \approx \pm(\gamma - i\Delta\beta)\left(1 + \frac{\kappa^2}{2(\gamma - i\Delta\beta)^2}\right) \qquad \gamma \gg \kappa$$

so that

$$S - (\gamma - i\Delta\beta) \cong -2(\gamma - i\Delta\beta)$$

$$S + (\gamma - i\Delta\beta) \cong \frac{-\kappa^2}{2(\gamma - i\Delta\beta)}$$

and (16.3-13) becomes

$$\frac{4(\gamma - i\Delta\beta)^2}{\kappa^2} e^{2SL} = -1 \tag{16.3-14}$$

Equating the phases on both sides of (16.3-14) results in

$$2\tan^{-1}\frac{(\Delta\beta)_m}{\gamma_m} - 2(\Delta\beta)_m L + \frac{(\Delta\beta)_m L\kappa^2}{\gamma_m^2 + (\Delta\beta)_m^2} = (2m+1)\pi \tag{16.3-15}$$

$$m = 0, \pm 1, \pm 2, \ldots$$

In the limit $\gamma_m \gg (\Delta\beta)_m, \kappa$, the oscillating mode frequencies are given by

$$(\Delta\beta_m)L \cong -\left(m + \frac{1}{2}\right)\pi \tag{16.3-16}$$

and since $\Delta\beta \equiv \beta - \beta_0 \approx (\omega - \omega_0)n_{\text{eff}}/c$

$$\omega_m = \omega_0 - \left(m + \frac{1}{2}\right)\frac{\pi c}{n_{\text{eff}}L} \tag{16.3-17}$$

We note that no oscillation can take place exactly at the Bragg frequency ω_0. The mode frequency spacing is

$$\omega_{m-1} - \omega_m \simeq \frac{\pi c}{n_{\text{eff}}L} \tag{16.3-18}$$

which is approximately the same as in a two-reflector resonator of length L. (See 4.1-10.)

The threshold gain value γ_m is obtained from equating the amplitudes in (16.3-14):

$$\frac{e^{2\gamma_m L}}{\gamma_m^2 + (\Delta\beta)_m^2} = \frac{4}{\kappa^2} \tag{16.3-19}$$

indicating an increase in threshold with increasing mode number m. This is also evident from the numerical gain plots (Figures 16-7 and 16-8). An important feature that follows from (16.3-19) is that the threshold gain for modes with the same $|\omega - \omega_0|$, or equivalently the same $|\Delta\beta|$, is the same. Thus two modes will exist with the lowest threshold, one on each side of ω_0. This property of DFB lasers is usually undesirable, and methods for obtaining single-mode operation are discussed in the last part of this section.[3] The periodic perturbation in semiconductor DFB lasers is achieved by incorporating a grating, usually in the form of a rippled interface, in the laser structure. This is achieved by interrupting the crystal growth at the appropriate stage and wet-chemical etching a corrugation into the topmost layer by

[3]High-speed (data rate) optical communication in fibers requires that the optical source put out a single frequency in order to minimize the temporal spread of the optical pulses with distance, which is caused by group velocity dispersion.

using an interferometrically produced photoresist mask [10]. Growth of a layer with a different index of refraction, or optical absorption on top of the rippled surface, results in the desired spatial modulation.

A diagram of a distributed feedback laser using a GaAs-GaAlAs structure is shown in Figure 16-9. The waveguiding layer, as well as that providing the gain (active layer), is that of p-GaAs. The feedback is provided by corrugating the interface between the p-$Ga_{.93}Al_{.07}As$ and p-$Ga_{.7}Al_{.3}As$, where the main index discontinuity responsible for the guiding occurs. Figure 16-12 shows an example of a periodic gain grating. The laser in this example is based on the quaternary $GA_{1-x}In_xAs_{1-y}P_y$ as the active region and InP as the high-energy gap, low index-cladding layer. The feedback is achieved by growing an extra-absorbing, i.e., low-energy gap, layer and then etching through a mask to leave behind a periodic array of absorbing islands.

The increase in threshold gain with the longitudinal mode index m predicted by (13.6-19) and by the plots of Figures 16-7 and 16-8 manifests itself in a high degree of mode discrimination in the distributed feedback laser.

It follows from (16.3-17) and (16.3-19) that the two lowest threshold modes are those with $m = 0$ and $m = -1$ and that they are situated symmetrically on either side of the Bragg frequency ω_0 just outside the bandgap.

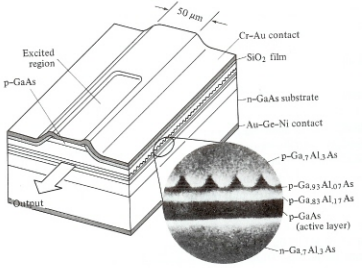

Figure 16-9 A GaAs–GaAlAs *cw* injection laser with a corrugated interface. The insert shows a scanning electron microscope photograph of the layered structure. The feedback is in third order ($\ell = 3$) and is provided by a corrugation with a period $\Lambda = 3\lambda_d/2 = 0.345$ μm. The thin (0.2 μm) p-$Ga_{.83}Al_{.17}As$ layer provides a potential barrier which confines the injected electrons to the active (p-GaAs) layer, thus increasing the gain. (After Reference [11].)

To understand why the basic DFB laser of Figure 16-6, in which the index of refraction is spatially periodic, does not oscillate at the Bragg frequency, consider Figure 16-10(a). Let the reflection coefficient of a wave (at ω) incident from the left on the plane $z = 0$ be r_2, and for a wave incident from the right, r_1. The reflectivity r_2 is given according to (16.3-11) by

$$r_1 = \frac{-\kappa \sinh SL_1}{(\gamma - i\Delta\beta)\sinh SL_1 - S\cosh SL_1} \qquad (16.3\text{-}20)$$

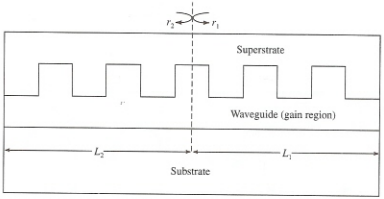

(a)

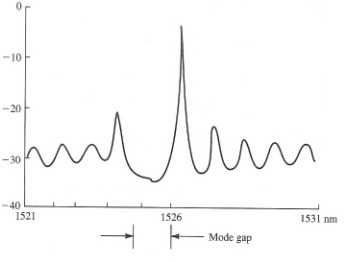

(b)

Figure 16-10 A periodic waveguide model used to derive Equation (16.3-12). (a) A periodic (DFB) GaInAsP waveguide laser. (b) The spontaneous emission spectrum below, but near, threshold of a DFB laser showing the mode gap. (c) A DFB laser with a phase shift section. (d) a "quarter wavelength shifted" DFB laser. (e) The spontaneous emission spectrum below threshold of a $\lambda/4$-shifted DFB laser. (Courtesy of P. C. Chen, ORTEL Corporation).

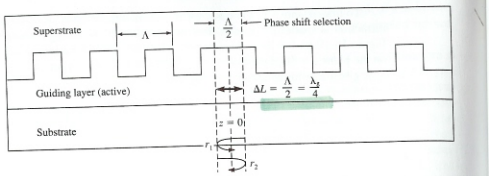

(c)

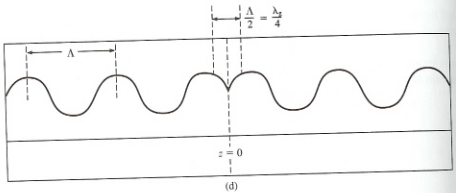

(d)

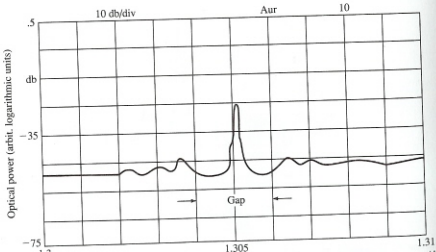

(e)

Figure 16-10 (*Continued*)

where

$$S = \sqrt{\kappa^2 + (\gamma - i\Delta\beta)^2}$$

$$\Delta\beta = \frac{\omega}{c} n_{\text{mode}} - \frac{\pi}{\Lambda} = (\omega - \omega_0)\frac{n_{\text{mode}}}{c} \tag{16.3-21}$$

and we used the fact that for an index perturbation of odd symmetry (in z), $\Delta n^2(z) \propto \sin(\eta z)$, the coupling coefficient κ given by (13.4-17) is a *real number*,[4] i.e., $\kappa_{ab} = \kappa_{ba} = \kappa$. The reflectivity r_1, "looking" to the left, is

$$r_1 = \frac{-\kappa \sinh SL_1}{(\gamma - i\Delta\beta)\sinh SL_1 - S\cosh SL_1}$$

The reason for the difference in sign between r_2 and r_1 is due to the fact that we chose, in (13.4-10), the index perturbation to have odd symmetry. An observer "looking" to the right sees $\Delta n(z) \propto \sin \eta z$, while an observer "looking" to the left will see a perturbation in index $\Delta n(z) \propto -\sin \eta z$. It follows that on resonance ($\Delta\beta = 0$), $r_1 r_2$ = negative number. The oscillation condition for a laser, on the other hand, is[5]

$$r_1(\omega) r_2(\omega) = 1 \tag{16.3-22}$$

It follows that the periodic index DFB laser cannot oscillate at the Bragg frequency ω_0 where $\Delta\beta = 0$. Oscillation thus takes place at the symmetrically situated frequencies shown in Figure 16-8. The two oscillation frequencies nearest the Bragg frequency require the lowest gain and are given, according to (16.3-17), by

$$\omega_0 \pm \frac{\pi c}{2 n_{\text{eff}} L} \tag{16.3-23}$$

The threshold gain for oscillation at these two frequencies, is, according to (16.3-24) and Figure 16-8, equal, so that they are in practice equally likely to oscillate. This situation is highly undesirable in practice, since it results in wavelength instabilities and spectral broadening. This is unacceptable, for example, in long-haul, high-data-rate fiber links where the increased spectral width due to multiwavelength oscillation was shown in Chapter 3 to limit the data rate due to pulse broadening by group velocity dispersion.

The existence of two such oscillating wavelengths is shown in the spectrum of Figure 16-10(b) as the two peaks on either side of the "gap."

A widely employed method [12] for forcing the DFB laser to oscillate preferentially at a single midgap frequency is shown in Figure 16-10(c, d). An extra section

[4]Had we chosen a reference plane other than $z = 0$, κ_{ab} will not be real, but since $\kappa_{ab} = \kappa^*_{ba}$, all the results remain the same.

[5]This is just a sophisticated way of saying that at steady state, the oscillation condition is equivalent to demanding that a wave launched, say, to the right, returns after one round trip with the same amplitude and the same phase (modulo $m2\pi$).